JOURNAL OF VIROLOGY, Sept. 1997, p. 6433–6444 Vol. 71, No. 9
0022-538X/97/$04.00+0

Translation Elongation Factor-1 Alpha Interacts with the 3′ Stem-Loop Region of West Nile Virus Genomic RNA

JERRY L. BLACKWELL† AND MARGO A. BRINTON*

Department of Biology, Georgia State University, Atlanta, Georgia 30302-4010

Received 6 January 1997/Accepted 24 May 1997

The conserved 3′-terminal stem-loop (3′ SL) of the West Nile virus (WNV) genomic RNA was previously used to probe for cellular proteins that may be involved in flavivirus replication and three cellular proteins were detected that specifically interact with the WNV 3′ SL RNA (J. L. Blackwell and M. A. Brinton, J. Virol. 69:5650–5658, 1995). In this study, one of these cellular proteins was purified to apparent homogeneity by ammonium sulfate precipitation and liquid chromatography. Amino acid sequence Western blotting, and supershift analyses identified the cellular protein as translation elongation factor-1 alpha (EF-1α). Competition gel mobility shift assays demonstrated that the interaction between EF-1α and WNV 3′ SL RNA was specific. Dephosphorylation of EF-1α by calf intestinal alkaline phosphatase inhibited its binding to WNV 3′ SL RNA. The apparent equilibrium dissociation constant for the interaction between EF-1α and WNV 3′ SL RNA was calculated to be 1.1×10^{-9} M. Calculation of the stoichiometry of the interaction indicated that one molecule of EF-1α binds to each molecule of WNV 3′ SL RNA. Using RNase footprinting and nitrocellulose filter binding assays, we detected a high-activity binding site on the main stem of the WNV 3′ SL RNA. Interaction with EF-1α at the high-activity binding site was sequence specific, since nucleotide substitution in this region reduced the binding activity of the WNV 3′ SL RNA for EF-1α by approximately 60%. Two low-activity binding sites were also detected, and each accounted for approximately 15 to 20% of the binding activity. Intracellular association between the host protein and the viral RNA was suggested by coimmunoprecipitation of WNV genomic RNA and EF-1α, using an anti-EF-1α antibody.

West Nile virus (WNV), a mosquito-borne member of the *Flavivirus* genus within the family *Flaviviridae*, has a single-stranded, positive-polarity RNA genome that is about 10.7 kb in length. The viral structural and nonstructural genes are expressed from a single open reading frame, and the resulting polyprotein is proteolytically cleaved into 10 mature viral proteins. The 3′ noncoding region (NCR) of the genomic RNA is approximately 650 nucleotides (nt) in length and contains several short conserved sequences and a predicted 3′-terminal stem-loop (SL) structure. Biochemical structure probing experiments confirmed the presence of a stable SL at the 3′ terminus of the WNV genomic RNA (12), and recently this 3′ sequence was shown to also contain a tertiary structure (56). Evidence from several laboratories support a role for the 3′-terminal sequences in flavivirus replication. The 3′ termini of all the mosquito- and tick-borne flavivirus genomes sequenced to date are predicted to form similar secondary (12, 20, 36, 38, 60, 66) and tertiary (56) structures despite little sequence homology. Although the lengths and sequences of the 3′ NCRs of 12 tick-borne encephalitis virus strains vary significantly, the 3′-terminal portion is highly conserved (64). Deletion and mutation analyses of the 3′ SL of dengue virus type 4 infectious cDNA clones demonstrated that the 3′-terminal nucleotides are required for virus replication (37). Collectively, these data support the hypothesis that the conserved 3′-terminal sequences and structures are required for flavivirus replication. Also, their location on the genome suggests that they may serve as promoters for the initiation of viral minus-strand RNA synthesis.

In some RNA virus systems, host proteins have been shown to be involved in viral RNA replication. Host proteins have been detected in the viral RNA replication complexes of bacteriophage Qβ (6, 31), brome mosaic virus (BMV) (51), influenza virus (46), Sindbis virus (3), and cucumber mosaic virus (24). In addition, a number of host proteins have been reported to interact in vitro with various putative viral RNA *cis*-acting elements previously shown to be associated with viral replication (15, 22, 29, 40, 41, 59, 67, 68). In two recent reports, host protein binding sites on viral RNAs were shown to colocalize with *cis*-acting sequences that were demonstrated to be required for viral replication. The U-rich *cis*-acting sequence located in the 3′ NCR of potato X virus was shown to specifically interact with two host proteins and to be required for virus replication (59). A similar correlation was demonstrated for a conserved 11-nt 3′-terminal sequence in mouse hepatitis virus genomic RNA that was required for both host protein binding and viral RNA replication (68). These data suggest that the interaction between host proteins and viral *cis*-acting elements is functionally relevant for the replication of viral RNAs.

The molecular identities of some of the host proteins that interact with either viral proteins or viral RNA *cis*-acting sequences have been reported. Elongation factor-1 alpha (EF-1α) interacts with the 5′ end of poliovirus genomic RNA and the aminoacylated 3′ end of turnip yellow mosaic virus genomic RNA (22, 25); translation elongation initiation factor-3 (eIF-3) interacts with the 3′ end of BMV genomic RNA and enhances BMV RNA replication (51); ribosomal protein S1, EF-Tu, and EF-Ts are components of the bacteriophage Qβ replicase complex (6, 31); La interacts with human immunodeficiency virus type 1, Sindbis virus, and vesicular stomatitis virus *cis*-acting RNA sequences (15, 49, 67); TAR RNA bind-

* Corresponding author. Mailing address: Georgia State University, Department of Biology, P.O. Box 4010, Atlanta, GA 30302-4010. Phone: (404) 651-3113. Fax: (404) 651-2509. E-mail: biomab@panther.gsu.edu.

† Present address: Department of Pathology, University of Alabama at Birmingham, Birmingham, AL 35294

A.

Primer name	Primer sequences
P1	CAGGAAACAGCTATGAC
P2	AGTATCCTGTGTTCTCGCAC
P3	[T7]-TGCACAACCAGCCACACGGC
P4	TTCTCGCACCACCAGCCACC
P5	[T7]-AGATCTTCTGCTCTGCACAACC
P6	[P2]-CCACCAGCCACCATTGTCGGCCGTGAGTGCCG
P7	[P2]-CCACCAGCCACGTAACACGGCGCACTGTGCCG
P8	AGTATCCTGTGTTCTCAAGCCACCAGCC
P9	[T7]-AGATCTTCTGCTCTTTGCAACCAGCC
P10	ACCAGCCACCATTGTCGGCGCAC
P11	TGACCGGCAGCAAAATG

B.

Primer pairs	3'SL RNA products
P1 + P2	RNA-1
P3 + P4	RNA-3
P5 + P2	RNA-4
P1 + P6	RNA-5
P1 + P7	RNA-6
P5 + P8	RNA-7
P9 + P2	RNA-8
P9 + P8	RNA-9
P5 + P4	RNA-10
P5 + P10	RNA-11
P1 + P11	RNA-12

FIG. 1. PCR primers used to generate DNA templates for RNA transcription in vitro. (A) The names and sequences (shown 5′ to 3′) of the primers used in this study for generating DNA templates for RNA transcription in vitro. Some of the primers include the T7 promoter sequence (GAATTCTAATACGACTCACTAT AGGG), designated [T7], or the primer 2 sequence, [P2], that is complementary to the 3′-terminal 20 nt of the WNV genomic RNA. The nucleotides that were substituted in the wild-type sequence are underlined. (B) Primer pairs used for PCR amplification of the DNA templates used for in vitro transcription of the different 3′ SL RNA probes and the names of the RNA products generated from each of the in vitro transcription reactions. RNA-1 corresponds to the wild-type sequence; RNA-3 to RNA-11 are deleted or mutated derivatives of the wild-type sequence.

ing protein interacts with a transactivating RNA element of human immunodeficiency virus type 1 (19); calreticulin interacts with a 3′ structure of rubella virus genomic RNA (42, 57); and heterogeneous nuclear ribonucleoprotein 1A interacts with human T-cell leukemia virus type 2 RNA regulatory elements (7). All of these host proteins except the TAR RNA binding protein and calreticulin normally interact with cellular RNA. The utilization of host proteins that normally interact with cellular RNA may be a characteristic that is common to the replication mechanisms of many RNA viruses.

Previously we detected three host proteins that specifically interact with the 3′ SL region of the WNV genomic RNA (8). In the present study, we report the purification and identification of one of these host proteins. We have mapped the binding site(s) for the protein on the WNV positive-polarity 3′ SL [(+)3′SL] RNA and quantified the interaction between WNV (+)3′SL RNA and the host protein. We also demonstrate that the host protein interacts with the WNV genomic RNA in infected cells, suggesting that this RNA-protein interaction is relevant to WNV replication.

MATERIALS AND METHODS

Cells and virus. BHK-21/WI2 cells (hereafter referred to as BHK cells) were used as the source of uninfected and infected cytoplasmic extracts (61). Confluent monolayers of BHK cells in T-150 flasks were infected with WNV, strain E101, at a multiplicity of infection of 1 as described previously (11). The preparation of a 10% (wt/vol) brain homogenate for the WNV stock pool used to infect the BHK cells was described previously (11). Cytoplasmic extracts from BHK cells were prepared at different times post infection as described below.

Synthesis of DNA templates for RNA transcription. The DNA templates used for in vitro RNA transcription reactions were generated by PCR from plasmid pWNV(+)3′SL as described previously (8). The sequences and combinations of primers used for the synthesis of the PCR products are shown in Fig. 1. PCR mixtures (100 μl) containing the pWNV(+)3′SL template (1 ng) and a pair of primers (100 pmol of each primer) were amplified with 2.5 U of *Taq* DNA polymerase as described by the manufacturer (Boehringer Mannheim). The thermal cycling parameters were as follows: 1 min at 95°C, 0.5 min at 50°C, and 0.5 min at 72°C, for a total of 30 cycles.

Preparation of RNA transcripts. WNV (+)3′SL RNA, which was used in the majority of these experiments, consisted of the 3′-terminal 111 nt of the WNV genomic RNA. Construction of the plasmid containing the WNV (+)3′SL RNA sequence was described previously (8). WNV (+)3′SL RNA (referred to as RNA-1 in some experiments) and its derivatives, RNA-3 through RNA-11 (see Fig. 8), were transcribed from the appropriate PCR products (Fig. 1B) in the presence of [α-^{32}P]GTP, using T7 RNA polymerase (50 U) as described by the manufacturer (Ambion), for 1 h at 37°C. The transcription reactions were stopped by the addition of DNase (1 U) for 15 min at 37°C, precipitated with ethanol, and gel purified as described previously (17). The precipitated RNAs were collected by centrifugation and resuspended into 100 μl of RNase-free storage buffer (100 mM sodium phosphate [pH 7.2], 300 mM potassium chloride, 5 mM EDTA, 5 mM dithiothreitol [DTT], 25% glycerol), and the amounts of radiolabeled RNAs produced were determined by scintillation counting. Radiolabeled RNA-2 was transcribed in vitro from pWNV(+)3′SL-trunc1 DNA digested with restriction enzyme *Sac*I as described previously (56). Unlabeled RNA-12 was transcribed from the appropriate PCR product (Fig. 1 and 7A) as described above except that unlabeled GTP (0.5 mM, final concentration) was substituted for radiolabeled GTP.

For some experiments, the RNA probe concentration was determined by assuming 99.9% scintillation counting efficiency for radioactive phosphorus and then converting counts per minute to disintegrations per minute. From this calculation, the molar concentration of radioactive G residues was first determined and then the molar concentration of WNV (+)3′SL RNA was derived for each preparation of RNA. In vitro transcription typically produced ^{32}P-WNV (+)3′SL RNA with a specific activity of approximately 1.2×10^7 cpm per pmol.

Gel mobility shift analyses. Uniformly ^{32}P-labeled WNV (+)3′SL RNA (10,000 cpm per reaction; 83 pM, final concentration) was incubated with a sample (2 μl) from each of the fractions from the purification procedure or with the purified host protein (10 to 25 ng) in reaction mixtures (10 μl) containing 1× binding buffer (20 mM sodium phosphate [pH 7.2], 60 mM potassium chloride, 1 mM EDTA, 1 mM DTT, 5% glycerol), poly(I-C) (50 ng/μl), poly(U) (50 ng/μl), and RNasin (10 U) for 30 min at room temperature. The RNA-protein complexes were resolved by nondenaturing polyacrylamide gel electrophoresis (PAGE) on a 6% polyacrylamide gel (150 V-h) in 0.5× Tris-borate-EDTA at 4°C and visualized by autoradiography. For the supershift gel mobility shift assay, purified EF-1α was incubated with ^{32}P-WNV (+)3′SL RNA in a binding reaction mixture (as described above) for 15 min at room temperature, and then anti-rabbit EF-1α antibody (described below) was added to the binding reaction mixture for 15 min at room temperature. For competition binding studies, the unlabeled competitor RNA was incubated with EF-1α in the binding reaction mixture 15 min before addition of ^{32}P-WNV (+)3′SL RNA. To determine the effect of dephosphorylation of EF-1α on its WNV (+)3′SL RNA binding activity, purified EF-1α was preincubated with calf intestinal alkaline phosphatase (CIP; 2 U) or with heat-inactivated CIP (2 U) for 30 min at 30°C in 1× binding buffer supplemented with 0.1 mM zinc chloride, which is required for CIP activity. For this experiment, CIP was inactivated by heating the enzyme to 100°C for 30 min. To determine the dissociation constant, binding reaction mixtures were prepared as described above except that the final concentration of purified EF-1α was varied from approximately 0.07 to 22.4 nM. RNA-protein complexes and unbound probe were then quantified by using a Bio-Rad GS-700 densitometer and Molecular Analyst software to establish the saturation binding curve. The data were then transformed to quantify the equilibrium dissociation constant and the stoichiometry of the RNA-protein interaction as described previously (35, 65).

Purification of the host protein. Approximately 10^9 BHK cells were harvested from T-225 tissue culture flasks, washed three times with ice-cold phosphate-buffered saline (PBS), resuspended into 20 ml of buffer A (50 mM sodium phosphate, 20% glycerol, 2 mM DTT [pH 7.5]), and incubated on ice for 15 min. Cells were lysed by Dounce homogenization, and the homogenate was centrifuged at $2,000 \times g$ for 15 min at 4°C to remove nuclei. Ammonium sulfate (solid) was slowly added to the cytoplasmic extract to a final concentration of 1.5 M. The extract was precipitated on ice for 30 min and centrifuged at $100,000 \times g$ for 1 h at 4°C. The supernatant from the 1.5 M ammonium sulfate step was diluted to 1.0 M ammonium sulfate with buffer A, passed through a 0.2-μm-pore-size filter, and loaded onto a phenyl-Superose HR5/5 column (Pharmacia) that was pre-equilibrated with buffer A containing 1.0 M ammonium sulfate. The supernatant

from the 1.5 M ammonium sulfate step was fractionated by a 40-ml gradient of 1.0 to 0 M ammonium sulfate in buffer A. Fractions (1.0 ml) were collected. The WNV (+)3′SL RNA binding activity eluted between 0.25 and 0 M ammonium sulfate. These fractions were pooled and dialyzed against two liters of buffer A containing 25% glycerol for 12 h at 4°C. The dialyzed protein sample was loaded onto a MonoQ HR5/5 column (Pharmacia) that was preequilibrated with buffer A. The WNV (+)3′SL RNA binding activity was detected in the flowthrough material from this column. The flowthrough material was applied directly to a MonoS HR5/5 (MS) column (Pharmacia) and was fractionated by a 40-ml gradient of 0 to 1.0 M NaCl in buffer A. The peak WNV (+)3′SL RNA binding activity eluted between 0.15 to 0.20 M NaCl. These fractions were pooled and concentrated approximately 40-fold with Centricon-10 microconcentrators (Amicon) and were stable for approximately 3 to 4 weeks when stored at −20°C in 20% glycerol.

At each step of the purification procedure, a sample (2.0 μl) of each fraction was assayed for WNV (+)3′SL RNA binding activity by using gel mobility shift assays as described above. Fractions with peak WNV (+)3′SL RNA binding activity were also analyzed by sodium dodecyl sulfate (SDS)-PAGE (12% polyacrylamide gel), and the protein concentrations were determined by a bicinchoninic acid protein assay (Pierce). The total amount of protein for each of the chromatography fractions is shown in Fig. 2A. The final protein concentration of the pooled and concentrated fractions from the MS column was approximately 25 μg/ml.

N-terminal amino acid sequence analyses. The purified host protein was cleaved with cyanogen bromide (32) and separated by SDS-PAGE (12% gel) at neutral pH as described previously (39). Following electrophoretic transfer to a polyvinyl difluoride membrane (0.2-μm pore size; Bio-Rad), selected peptide fragments were subjected to Edman degradation chemical sequencing at the Georgia State University DNA/Protein Core Facility, Atlanta. Trypsin fragments generated from the host protein were separated by high-pressure liquid chromatography, analyzed by mass spectroscopy, and subjected to Edman degradation chemical sequencing at the Wistar Protein Microsequencing Facility, Philadelphia, Pa. The amino acid sequences obtained were used to search the Swiss-Prot protein sequence database with the BLAST sequence similarity searching program (default filtering) at the National Center for Biotechnology Information (Internet address, http;//www.ncbi.nlm.nih.gov).

Western blotting analysis for detection of EF-1α. Goat polyclonal antibody against rabbit reticulocyte EF-1α was made by injecting a goat with rabbit EF-1α (approximately 1 mg) in 1 ml of Freund's adjuvant. The presence of anti-EF-1α immunoglobulin G in the goat serum was confirmed by Ouchterlony double diffusion. Goat anti-EF-1α antibody and purified rabbit EF-1α (26) were gifts from William W. Merrick, Case Western Reserve University, Cleveland, Ohio. BHK cells from a T-150 flask were lysed by Dounce homogenization, and the extract was centrifuged at 2,000 × *g* for 15 min at 4°C to remove nuclei and cellular debris. The resulting supernatant (designated S2 supernatant) and purified host protein were electrophoresed on an SDS–12% polyacrylamide gel and electrophoretically transferred to a nitrocellulose membrane (0.2-μm pore size; Micron Separations, Inc.). The membrane was blocked with 5% powdered milk in PBS, washed (three times for 10 min each) with PBS containing 1% Triton X-100 (PBS-TX), and probed with goat anti-EF-1α antibody for 1 h at room temperature with constant rocking. The membrane was then washed with PBS-TX, probed with horseradish peroxidase-conjugated antigoat immunoglobulin G antibody, and visualized with a 3,3′-diaminobenzidine substrate detection kit (Vector Laboratories).

UV-induced cross-linking of RNA and protein. A sample (approximately 50 ng of total protein) of the pooled and concentrated fractions from the MS column was incubated with ^{23}P-WNV (+)3′SL RNA in a binding reaction mixture as described above. The binding reaction mixture was incubated for 30 min at room temperature and then transferred to an ice bath. The binding reaction mixture was irradiated (250 mJ) in a UV chamber (GS Gene Linker; Bio-Rad). After UV irradiation, RNase T_1 (2.5 U) was added to the binding reaction mixture for 15 min at 37°C to digest unprotected or unbound RNA. The UV cross-linked products were boiled in Laemmli sample buffer (30) containing 1% SDS for 3 min and analyzed by SDS-PAGE (12% gel). The gel was fixed in 7% acetic acid and dried, and the UV cross-linked products were visualized by autoradiography.

Northwestern blotting analysis of RNA binding protein. A sample (approximately 250 ng of total protein) of the pooled and concentrated fractions from the MS column was denatured and renatured on a solid support membrane and then probed with ^{32}P-WNV (+)3′SL RNA as described previously (8). Briefly, the protein sample was separated by SDS-PAGE (12% gel) and then electrophoretically transferred to a nitrocellulose membrane (0.22-μm pore size; Micron Separations). The membrane was blocked with PBS containing 5% dry milk and 1 mM DTT for 1 h and then was washed with 1× HBB (25 mM HEPES-KOH [pH 7.5], 25 mM NaCl, 5 mM $MgCl_2$, 1 mM DTT). Proteins were denatured and slowly renatured by consecutive washes (10 min each) with 6 (two times), 3, 1.5, 0.75, 0.375, and 0.187 M guanidine hydrochloride in 1× HBB. The membrane was washed once with 1× HBB and twice with HYB100 (20 mM HEPES-KOH [pH 7.5], 100 mM KCl, 2.5 mM $MgCl_2$, 0.1 mM EDTA, 0.05% Nonidet P-40, 1 mM DTT). ^{32}P-WNV (+)3′SL RNA in HYB100 (approximately 10^5 cpm/ml) was incubated with the renatured membrane-bound proteins for 1 h at room temperature and then for 6 h at 4°C. Unbound probe was removed from the membrane by three washes (10 min) with HYB100, and the membrane was visualized by autoradiography at −70°C.

RNase footprinting analysis. RNA-12, which included the 111 nt of RNA-1 plus a plasmid-derived 3′-terminal addition of 28 nt, was used to map the RNA-protein interaction by the RNase footprinting-primer extension method as described previously (53), with some modifications. Briefly, RNA-12 (25 ng) and γ-^{32}P-labeled 5′ end-labeled primer 11 (50 pmol; Fig. 1 and 7A) were annealed in 1× binding buffer (10.0 μl) by heating to 70°C for 2 min and then slow cooling to room temperature (approximately 20 min). Primer 11 was complementary to the 3′-terminal 18 nt of the plasmid-derived sequence and was located 10 nt downstream from the 3′ terminus of the WNV sequence in RNA-12 (see Fig. 7A). The annealed RNA-primer mixture was then incubated in the presence or absence of purified EF-1α (100 ng) for 30 min at room temperature. RNase A (10^{-1} to 10^{-3} U/μl) was added, and the reaction mixture was incubated for an additional 15 min at 30°C. The reaction mixture was extracted with phenol-chloroform and precipitated with ethanol. The RNA was pelleted by centrifugation and resuspended into RNase-free H_2O (10 μl). cDNA was then synthesized in a reaction mixture (20 μl) with SuperScript II-RNase H^- reverse transcriptase at 42°C for 1 h as recommended by the manufacturer (GibcoBRL-Life Technologies). The reverse transcription (RT) reaction was terminated by the addition of an equal volume of stop solution (95% formamide, 20 mM EDTA, 0.05% bromophenol blue, 0.05% xylene cyanol FF), and the mixture was heated for 3 min at 80°C and analyzed on a 7 M urea–10% polyacrylamide gel. Undigested RNA-12 was sequenced with primer 11, using an RT RNA sequencing kit as described by the manufacturer (United States Biochemical).

Nitrocellulose filter binding assay. ^{32}P-labeled RNA-1 to RNA-11 (100,000 cpm; approximately 80 to 160 pM) were separately incubated with EF-1α (100 ng; approximately 20 nM) in binding reaction mixtures (100 μl) that were prepared as described above except that the binding reaction mixtures were scaled up 10-fold. EF-1α that was heat inactivated by heating to 100°C for 30 min was substituted for active EF-1α in binding reaction mixtures to determine the amount of nonspecific binding of [^{32}P]RNA to the nitrocellulose membrane. After incubation for 30 min at room temperature, 90% of each binding reaction mixture (90 μl) was vacuum filtered through a nitrocellulose membrane (0.22-μm pore size; NitroBind; Micron Separations) that was preequilibrated with 1× binding buffer. The membrane-bound material was washed two times with 250 μl of binding buffer. To quantify the total amount of [^{32}P]RNA in each binding reaction mixture, the remaining 10% of the binding reaction mixture (10 μl) was pipetted directly onto the nitrocellulose membrane and dried without vacuum filtering or washing. The nitrocellulose membrane was dried under a heat lamp and autoradiographed for approximately 1 h. The nitrocellulose membrane was also phosphorimaged (Fujix BAS1000 phosphorimager), and the amounts of total and bound [^{32}P]RNAs in each binding reaction mixture were quantified by using MacBAS version 2.00 software. Values obtained for the amounts of total and bound [^{32}P]RNAs were adjusted according to the volumes applied to the nitrocellulose membrane.

Immunoprecipitation of WNV RNA. WNV genomic RNA was coimmunoprecipitated with an anti-EF-1α antibody as described previously (57), with some modifications. Briefly, one T-150 flask of mock-infected and one of WNV-infected (multiplicity of infection of 1) BHK cells were harvested 16 h postinfection, washed three times with cold PBS, and resuspended into 1× binding buffer (10^8 cells per ml). An S2 supernatant, prepared as described above, was centrifuged at 100,000 × *g* for 1 h at 4°C. The resulting supernatant (designated S100 supernatant) was collected and incubated either with Sepharose A CL-4B beads alone or with Sepharose A CL-4B beads coupled to the anti-rabbit EF-1α antibody or to a control goat antibody (goat anti-mouse IgG immunoglobulin G; Pierce). Coupling of the antibodies to Sepharose A CL-4B beads (Pharmacia) was done as described previously (58). After centrifugation at 2,000 × *g* for 2 min to pellet the antibody-coupled Sepharose A beads, the immunoprecipitate was washed three times with 1× binding buffer containing 0.1% Triton X-100. The final immunoprecipitate was resuspended into RNase-free H_2O (50 μl), heated to 60°C for 30 min to release any bound RNA, and centrifuged at 10,000 × *g* for 10 min. An aliquot (5 μl) of the resulting supernatant was added to RNase-free H_2O (5 μl) containing primer 2 (50 pmol) (Fig. 1), which was complementary to the 3′-terminal 20 nt of the WNV genomic RNA. The WNV RNA and primer 2 were annealed, and cDNA was synthesized in an RT reaction mixture (20 μl) as described for the RNase footprinting assay (above). The cDNA was then subjected to PCR amplification with *Taq* DNA polymerase as described by the manufacturer (Boehringer Mannheim), using primer 2 (100 pmol) and a genomic-sense primer (100 pmol; 5′-ATATTGATACCTGGGA-3′) that was located 114 nt upstream from the WNV 3′ terminus. The PCR mixtures were thermal cycled (40 times) as follows: 1 min at 95°C, 0.5 min at 55°C, and 1.0 min at 72°C. The PCR products were analyzed on a 6% polyacrylamide gel and stained with ethidium bromide, and the 114-bp PCR product was eluted from the gel. The gel-purified 114-bp RT-PCR product was analyzed by *Bgl*II restriction enzyme digestion and was directly sequenced with a Sequenase version 2.0 DNA sequencing kit (United States Biochemical), using primer 2.

Prediction of RNA secondary structure. The optimal secondary structures based on minimum free energies for each of the wild-type and mutated or truncated 3′ SL RNAs were predicted by the method of Zuker (69), using the FoldRNA program in the Genetics Computer Group sequence analysis software package (version 8).

A.

Fraction	Total protein (μg)	Specific activity	Fold enrichment
Starting cytoplasmic extract	31600	1	(-)
Ammonium sulfate precipitation	23600	9.8	~10
Hydrophobic chromatography	1260	3672	3.6×10^3
Anion exchange chromatography	840	5520	5.5×10^3
Cation exchange chromatography	5	24400	2.4×10^4

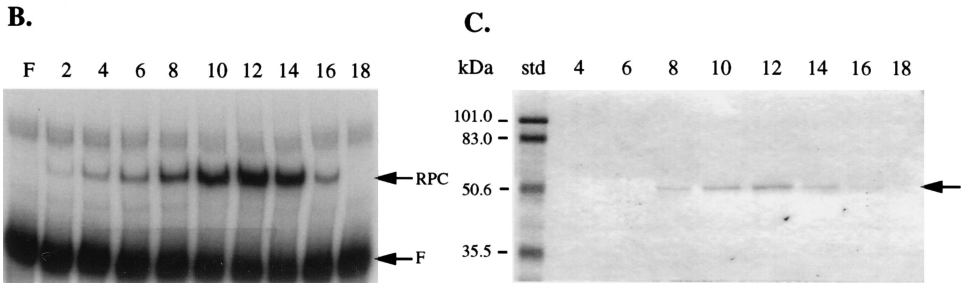

FIG. 2. Purification of a 50-kDa host protein that interacts with the WNV (+)3′SL RNA. (A) Summary of the purification steps. An S2 supernatant from a BHK extract was fractionated by ammonium sulfate precipitation and liquid chromatography as described in Materials and Methods. The protein concentration of each fraction was determined by the bicinchoninic acid protein assay. The specific activity at each step of the purification procedure was monitored by using a standardized gel mobility shift assay as shown in Fig. 2B. The specific activity was defined as the amount of protein required in the binding reaction mixture to shift 1 pmol of WNV (+)3′SL RNA divided by the total amount of protein in the respective fraction. The fold enrichment was defined as the specific activity of the fraction from each step of the purification procedure divided by the specific activity of the initial starting material. (B) Analysis of the RNA binding activity of fractions from the cation exchange column. Samples from every other fraction from 2 to 18 were incubated with ^{32}P-WNV (+)3′SL RNA, and the RNA-protein complexes (RPC) were resolved by nondenaturing PAGE (6% gel). The free probe (F) and fraction numbers are indicated at the top. (C) Protein analysis of fractions from the cation-exchange column. A sample (100 μl) of each fraction was precipitated with 50% acetone–50% methanol and analyzed by SDS-PAGE (12% gel) followed by Coomassie blue staining. The arrow indicates the position of the 50-kDa protein. Fraction numbers are indicated at the top. The molecular masses of the protein standards (std) are indicated on the left.

Production of computer-generated digitized images. Autoradiographs of the gels or membranes (i.e., Fig. 2B, 2C, 3B, 4A, 4B, 5A, 6B, 8A, and 9A) were scanned on a ScanJet IIcx flatbed scanner (400-dots-per-in. resolution; Hewlett-Packard) driven by Deskscan II version 2.1 software on a Quadra 840AV computer (Apple Computer, Inc.). The digitized images were enhanced by using Adobe Photoshop version 3.0.5 software and output with a Phaser 440 printer (Tektronix).

RESULTS

Purification of a host protein that interacts with the WNV (+)3′SL RNA. Because of its probable *cis*-acting function in RNA replication, the WNV (+)3′SL RNA was selected as a probe for detecting host proteins that may be associated with WNV replication. We previously reported the detection of three host proteins that interacted with WNV (+)3′SL RNA by using gel mobility shift and UV-induced cross-linking assays (8). As the next step in analyzing these proteins, liquid chromatography protocols are being developed to purify and identify each of these host proteins. A summary of the protocol used to purify one of these host proteins is shown in Fig. 2A. During each step of the purification protocol, the RNA binding activity of each fraction was determined by a gel mobility shift assay using radiolabeled WNV (+)3′SL RNA as the probe. The binding reaction mixtures contained sufficient competitor RNA to inhibit nonspecific interactions and a constant amount (1 pmol) of ^{32}P-WNV (+)3′SL RNA so that the specific activities of individual fractions could be quantified and compared during the purification procedure.

Cytoplasmic extracts prepared from approximately 10^9 BHK cells contained approximately 30 mg of total protein (Fig. 2A). Proteins in the cytoplasmic extract were initially fractionated by precipitation with 1.5 M ammonium sulfate. About 75% of the WNV (+)3′SL RNA binding activity detected in the original cytoplasmic extract remained in the supernatant fraction after ammonium sulfate precipitation. The proteins in the ammonium sulfate supernatant fraction were then subjected to additional purification by liquid chromatography using hydrophobic, anion-exchange, and cation-exchange media. Fractions having WNV (+)3′SL RNA binding activity were pooled and loaded onto the next column of the purification procedure. Under the buffer conditions used for the purification procedure, the previously detected 50-kDa WNV (+)3′SL RNA binding protein (8) did not bind to the anion-exchange column. However, approximately 33% of the other cell proteins bound to the anion-exchange column, making this negative selection step effective for enrichment of the 50-kDa host protein. In addition, this column removes cellular RNAs, such as transfer and ribosomal RNAs, which are natural substrates for RNA binding proteins. The flowthrough material from the anion-exchange column was directly loaded onto a cation-exchange column. Fractions 8 through 14 from the cation-exchange column had WNV (+)3′SL RNA binding activity (Fig. 2B). SDS-PAGE analysis of the same fractions detected a predominant Coomassie blue-stained protein with a molecular mass of approximately 50 kDa (Fig. 2C). The results from these two analyses demonstrated a direct correlation between the level of WNV (+)3′SL RNA binding activity and the amount of the 50-kDa protein in each fraction, indicating that the highly purified 50-kDa protein was responsible for the RNA binding activity associated with fractions 8 through 14.

Identification of the purified host protein. Initial attempts to identify the purified 50-kDa protein by Edman degradation chemical sequencing were unsuccessful presumably due to a blocked N terminus. Subsequently, cyanogen bromide and trypsin fragments were generated from the purified protein and sequenced as described in Materials and Methods. The five amino acid sequences obtained from the cyanogen bromide and trypsin fragments (Fig. 3A) were identical to the sequences of human and Chinese hamster EF-1α (GenBank accession no. P04720 and P20001, respectively). The BHK cells used in these experiments were derived from Syrian hamsters.

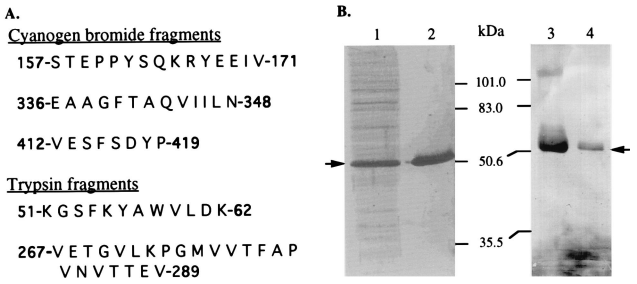

FIG. 3. Identification of the 50-kDa protein. (A) Amino acid sequence analyses of the 50-kDa protein. Cyanogen bromide and trypsin fragments of the 50-kDa protein were generated, purified, and subjected to Edman degradation chemical sequencing. The resulting five amino acid sequences were used to search the SwissProt database. Each peptide mapped to a different region of the amino acid sequence of Chinese hamster EF-1α, and the positions of the peptide fragments are indicated by the numbers at the ends of the amino acid sequences. (B) Western blotting analysis of the 50-kDa protein. Protein samples were electrophoresed on an SDS–12% polyacrylamide gel, transferred to a nitrocellulose membrane, and immunoblotted with anti-rabbit EF-1α antibody. Lanes: 1, BHK S2 supernatant (5μg); 2 and 4, purified 50-kDa protein from BHK cells (400 and 200 μg, respectively); 3, purified rabbit EF-1α (500 μg). The molecular masses of the protein standards are indicated. Arrows, EF-1α.

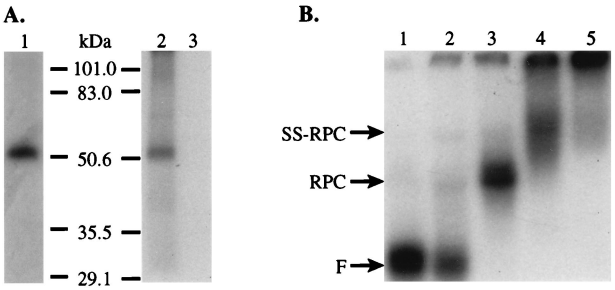

FIG. 4. Further characterization of the 50-kDa protein. Fractions 8 to 14 from the MS column (Fig. 2) were pooled and concentrated approximately fivefold. (A) A sample of the pooled MS fractions was analyzed by Northwestern blotting and UV-induced cross-linking assays. Lanes: 1, pooled MS fractions were separated by SDS-PAGE (12% gel), transferred to nitrocellulose, renatured, and probed with ^{32}P-WNV (+)3′SL RNA; 2 and 3, pooled MS fractions were cross-linked to ^{32}P-WNV (+)3′SL RNA, incubated with RNases T_1 and A, separated by SDS-PAGE (12% gel), and visualized by autoradiography; 3, pooled fractions were treated as described for lane 2 except that it was not irradiated with UV light. The sizes of the molecular weight standards are indicated. (B) Supershift gel mobility shift assay of the pooled MS fractions. Binding reaction mixtures were separated by nondenaturing PAGE (6% gel) and visualized by autoradiography. Lanes: 1 and 2, free ^{32}P-WNV (+)3′SL RNA in the absence and presence, respectively, of anti-EF-1α antibody diluted 1:250; 3, ^{32}P-WNV (+)3′SL RNA incubated with the pooled MS fractions; 4 and 5, ^{32}P-WNV (+)3′SL RNA incubated with the pooled MS fraction in the presence of anti-EF-1α antibody diluted 1:500 and 1:250, respectively. The positions of the free WNV (+)3′SL RNA probe (F), the RNA-protein complex (RPC), and the supershifted RNA-protein complex (SS-RPC) are indicated (arrows).

In addition, these amino acid sequences mapped to different regions that were broadly distributed across the known sequences of EF-1α.

EF-1α belongs to a superfamily of genes with a high degree of nucleotide and amino acid sequence similarity (reference 2 and references therein). Within this superfamily, the EF-1α proteins from different eukaryotic species are antigenically cross-reactive. Western immunoblotting analysis was used to confirm the identity of the purified 50-kDa protein (Fig. 3). Polyclonal goat anti-rabbit EF-1α antibody detected EF-1α purified from rabbit reticulocytes and the 50-kDa protein purified from BHK cells (Fig. 3B, lanes 3 and 4, respectively). The 50-kDa protein was also detected in the cytoplasmic S2 supernatants from BHK cells (Fig. 3B, lane 1). A control goat antibody did not react with either of the purified EF-1α proteins (data not shown). The purified 50-kDa protein that binds the WNV (+)3′SL RNA was therefore identified as the translation factor EF-1α, based on its estimated size, its homology with the amino acid sequences obtained from other mammalian EF-1α proteins, and its antigenic cross-reactivity with antibodies elicited by rabbit EF-1α. Since no mixed polypeptide sequences were detected during the N-terminal amino acid sequence analyses, it is likely that the 50-kDa band contained only EF-1α.

Confirmation that the 50-kDa protein is responsible for the WNV (+)3′SL RNA binding activity and is EF-1α. Since it was possible that trace amounts of another protein were responsible for the RNA binding activity observed in the fractions from the cation-exchange column, additional experiments were performed to confirm that the 50-kDa protein was the WNV (+)3′SL RNA binding protein. Fractions 8 through 14 from the cation-exchange column (Fig. 2B) were pooled and concentrated approximately 40-fold. A sample (approximately 2 μg of total protein) of the pooled fractions was subjected to SDS-PAGE (12% gel) and silver stained to detect the protein(s) present (data not shown). Only the 50-kDa protein band was detected. Northwestern blotting (Fig. 4A, lane 1) and UV-induced cross-linking (Fig. 4A, lane 2) assays were performed to determine the size of the protein in the pooled fractions that interacted with WNV (+)3′SL RNA. Both assays detected only a 50-kDa protein. The pooled fractions were also subjected to a gel mobility shift assay in the presence of the anti-rabbit EF-1α antibody. The characteristic RNA-protein complex formed between ^{32}P-WNV (+)3′SL RNA and the 50-kDa protein was observed (Fig. 4B, lane 3) when no antibody was included in the binding reaction mixture. The electrophoretic mobility of the RNA-protein complex was retarded by addition of the anti-rabbit EF-1α antibody (Fig. 4B, lane 4). At higher concentrations, the anti-rabbit EF-1α antibody apparently caused aggregation of the RNA-protein complex, since the complex did not migrate out of the well of the polyacrylamide gel (Fig. 4B, lane 5). Addition of the same amounts of the control goat antibody did not retard the electrophoretic migration or cause aggregation of the RNA-protein complex (data not shown). These data indicate that a 50-kDa protein in the pooled fractions interacts with WNV (+)3′SL RNA (Fig. 4A) and that this protein is EF-1α, since the anti-rabbit EF-1α antibody caused a supershift in the migration of the RNA-protein complex (Fig. 4B, lane 4).

Characterization of the RNA binding activity of EF-1α. The specificity of the interaction between purified EF-1α and WNV (+)3′SL RNA was determined by a competition gel mobility shift assay (Fig. 5). EF-1α was incubated with ^{32}P-WNV (+)3′SL RNA in binding reaction mixtures containing different competitor RNAs. RNA-protein complex formation was reduced proportionally by adding increasing amounts of specific competitor RNA [i.e., unlabeled WNV (+)3′SL RNA] to the binding reactions mixtures (Fig. 5A, lanes 3 to 6). Low amounts (between 30 and 60 ng) of the specific competitor completely inhibited the interaction between EF-1α and WNV (+)3′SL RNA (Fig. 5A, lanes 5 and 6, respectively). Much higher amounts (250 or 500 ng) of the various nonspecific competitor RNAs had essentially no effect on the formation of the RNA-protein complexes (Fig. 5A, lanes 7 to 10). These data indicate that the RNA-protein complex that is formed between EF-1α and WNV (+)3′SL RNA is the result of specific interactions.

It has been observed that EF-1α is differentially phosphorylated as it cycles between active and inactive forms during

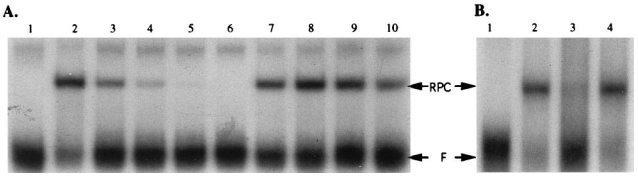

FIG. 5. Characterization of the interaction between EF-1α and WNV (+)3′SL RNA. (A) Competition gel mobility shift analysis to determine the specificity of the interaction between EF-1α and ^{32}P-WNV (+)3′SL RNA. Lanes: 1, free WNV (+)3′SL RNA; 2, RNA-protein complex formed in the absence of competitor RNA; 3 to 6, RNA-protein complex formation in the presence of 7.5, 15, 30, and 60 ng of specific competitor [i.e., WNV (+)3′SL RNA], respectively; 7 to 10, RNA-protein complex formation in the presence of nonspecific competitor tRNA (250 ng), poly(I-C) (500 ng), *Torula* yeast RNA (250 ng), and poly(U) (500 ng), respectively. Arrows indicate the positions of the free WNV (+)3′SL RNA (F) and the RNA-protein complex (RPC) formed between EF-1α and WNV (+)3′SL RNA. (B) Gel mobility shift analysis of the effect of dephosphorylation on the WNV (+)3′SL RNA binding activity of EF-1α. Lanes: 1, free WNV (+)3′SL RNA; 2, RNA-protein complex formed after preincubation of EF-1α in 1× CIP reaction buffer in the absence of CIP; 3, RNA-protein complex formed after preincubation of EF-1α in 1× CIP reaction buffer in the presence of CIP; 4, RNA-protein complex formed after preincubation of EF-1α in 1× CIP reaction buffer in the presence of heat-inactivated CIP.

protein translation and that the extent of EF-1α phosphorylation correlates with the rate of protein translation activity both in vitro and in vivo (48, 62, 63). The role of phosphorylation in the interaction between EF-1α and WNV (+)3′SL RNA was assessed. Purified EF-1α was dephosphorylated at phosphoserine and/or phosphothreonine residues with CIP (55), and then its ability to interact with WNV (+)3′SL RNA was determined by a gel mobility shift assay. The binding activity of EF-1α was inhibited following dephosphorylation by CIP (Fig. 5B, lane 3). Preincubation of EF-1α in 1× CIP reaction buffer without CIP and with heat-inactivated CIP did not inhibit the viral RNA binding activity of EF-1α (Fig. 5B, lanes 2 and 4, respectively). These data suggest that the WNV (+)3′SL RNA binding activity of EF-1α requires phosphorylation.

Determination of the dissociation constant for the RNA-protein complex. To determine whether the interaction was in the physiological range, the strength of the interaction between EF-1α and WNV (+)3′SL RNA was quantified by a gel mobility shift assay. Increasing amounts of purified EF-1α were titrated into binding reaction mixtures, and the amount of RNA-protein complex that formed was quantified (Fig. 6A). A theoretical saturation binding curve was generated by plotting the percent WNV (+)3′SL RNA bound versus the concentration of EF-1α in the binding reaction mixture (Fig. 6B). Based on the theoretical saturation binding curve, the equilibrium dissociation constant (K_d) was estimated to be 2.1 nM. The data were then transformed to calculate the K_d as described previously (35, 65). The K_d of the interaction between EF-1α and WNV (+)3′SL RNA was 1.1 nM, as determined from the plot of log[bound RNA]/[unbound RNA] versus log[EF-1α] (Fig. 6B, inset). Under conditions where the binding protein is in high molar excess relative to the RNA probe concentration, the slope of the line reflects the ratio of EF-1α molecules to WNV (+)3′SL RNA molecules in each RNA-protein complex. The slope of the line was calculated to be 1.3, demonstrating that approximately one EF-1α molecule binds to each WNV (+)3′SL RNA molecule. Similar K_d and slope values were obtained from five independent experiments with standard deviations of ±3 nM and ±0.08, respectively. The low K_d value indicates that this interaction is physiologically feasible.

Mapping the EF-1α binding site(s) on the WNV (+)3′SL RNA by RNase footprinting. Recognition elements on the WNV (+)3′SL RNA were mapped to gain a further understanding of the interaction between EF-1α and WNV (+)3′SL RNA. RNA-12, which included 111 nt of the WNV (+)3′SL sequence plus a 3′-terminal addition of 28 nt derived from the plasmid, was used to map the RNA-protein interaction (Fig. 7A). Following RNase digestion of RNA-12 in the presence or absence of purified EF-1α, the digestion products were analyzed by a modified primer extension technique (Fig. 7) (53). A region located between 5′-C_{47} and A_{50}-3′ in RNA-12 was protected from RNase digestion when EF-1α was present in the binding reaction mixture (Fig. 7B, lanes 4 to 6) but was susceptible to RNase digestion when EF-1α was absent from the binding reaction mixture (Fig. 7B, lanes 1 to 3). The identified protected region may not precisely define the nucleotides that contact EF-1α, since some of these nucleotides could have been protected by steric hindrance. However, the observed protected region would be close to the site to which EF-1α binds on RNA-12 and could contain some of the contact nts. Since much of the WNV (+)3′SL RNA structure is double

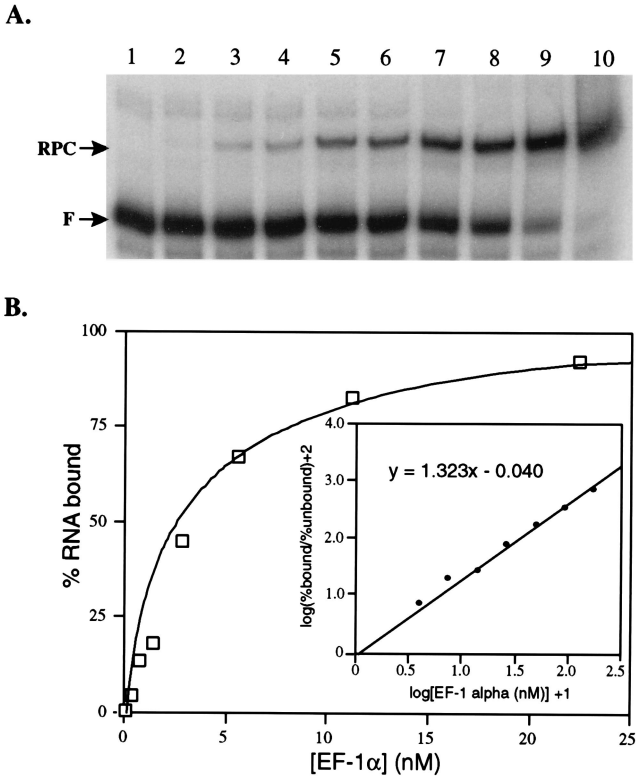

FIG. 6. Quantification of the interaction between EF-1α and the WNV (+)3′SL RNA. (A) Increasing amounts of EF-1α were incubated with a constant amount of ^{32}P-WNV (+)3′SL RNA, and the RNA-protein complexes (RPC) were analyzed by a gel mobility shift assay. Lanes: 1, free WNV (+)3′SL RNA; 2 to 10, WNV (+)3′SL RNA incubated with 0.07, 0.15, 0.35, 0.7, 1.4, 2.8, 5.6, 11.2, and 22.4 nM EF-1α, respectively. An autoradiograph of the dried gel was scanned with a Bio-Rad GS-700 densitometer (1,200 dots per in., 16-bit pixel depth), and the amounts of bound and unbound ^{32}P-WNV (+)3′SL RNA were quantified by using Molecular Analyst software. (B) The percent ^{32}P-WNV (+)3′SL RNA bound was plotted against the concentration of EF-1α to generate a theoretical saturation binding curve of the gel shown in panel A. The data point for lane 2 is superimposed on the data point for lane 3. The K_d was estimated to be 2.1 nM from the saturation binding curve. In the inset, the data from the saturation binding curve were transformed as described previously (35, 65), and the K_d was determined to be 1.2 nM. The endmost data points (from panel A, lanes 2 and 10) were discarded from this data set. The stoichiometry of the interactions, as determined by the slope of the line, was 1.0:1.3. The K_d and slope values were obtained from five independent experiments with standard deviations of ±3 nM and ±0.08, respectively.

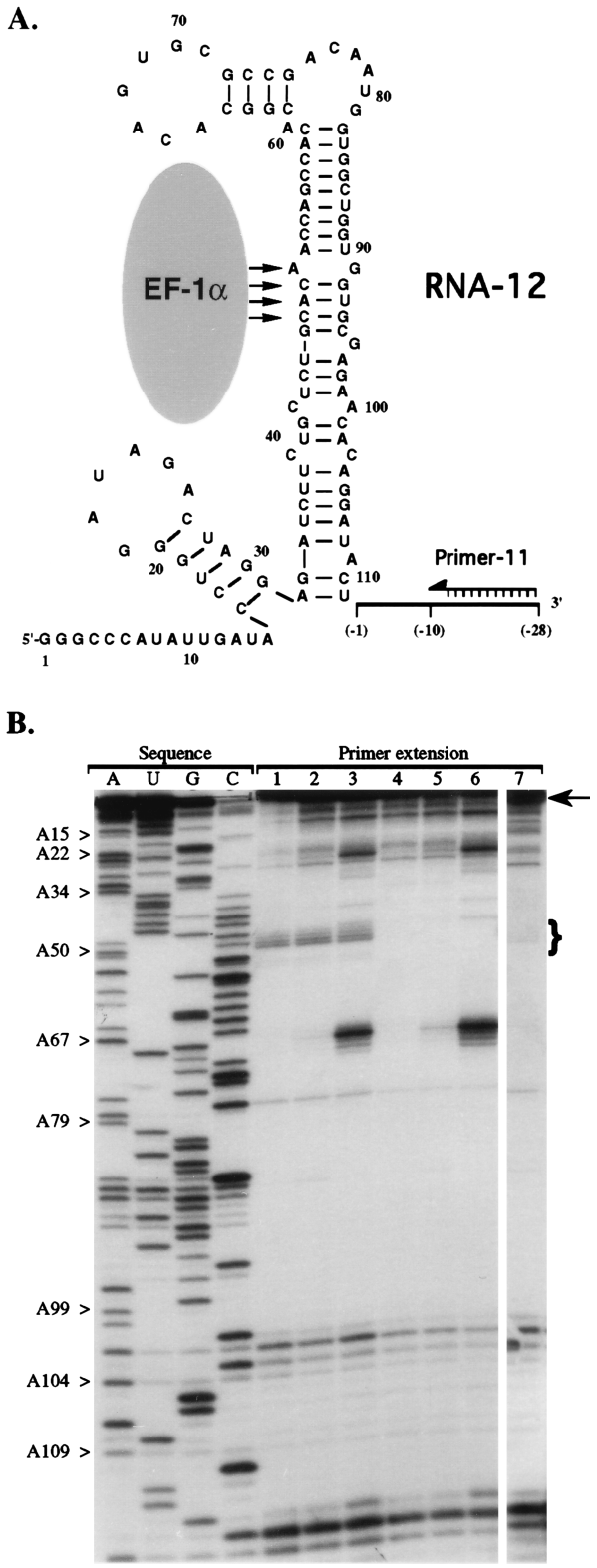

FIG. 7. RNase footprint of the EF-1α binding site on the WNV (+)3′SL RNA. (A) Diagram of RNA-12 used in the RNase footprinting experiment. RNA-12 contained the 3′-terminal nucleotides of the WNV genomic RNA, numbered 1 to 111 and oriented 5′ to 3′, and contained 28 plasmid-derived nucleotides, which were designated (−1) to (−28). RNA-12 was digested with RNase in the presence or absence of EF-1α, and then 5′-γ^{32}P-labeled primer 11, which is complementary to nt (−10) to (−28), was extended by reverse transcriptase. The primer extension cDNA products were then analyzed on a 7 M urea–12% polyacrylamide gel. The arrows indicate the region protected by EF-1α from RNase digestion. (B) Autoradiograph of the primer extension products. Lanes: 1 to 3, primer extension products produced in the absence of EF-1α after digestion of RNA-12 with RNase A (10^{-1}, 10^{-2}, and 10^{-3} U/μl; respectively); 4 to 6, primer extension products produced in the presence of EF-1α after digestion of RNA-12 with RNase A (10^{-1}, 10^{-2}, and 10^{-3} U/μl; respectively); 7, primer extension product produced from undigested RNA-12 in the presence of EF-1α. The sequencing reaction products obtained with RNA-12 as the template and primer 11 are shown in the first four lanes. The arrow indicates the position of the full-length primer extension product, and the brace (right) indicates the region in RNA-12 that was protected from RNase cleavage by EF-1α. The positions of selected A residues in the RNA-12 sequence are indicated on the left for reference.

stranded and therefore resistant to digestion with the single-strand-specific RNase, RNase A, we cannot rule out the possibility that there are other sites of interaction between EF-1α and WNV (+)3′SL RNA that were not detected by the RNase footprinting method used.

Mapping the EF-1α binding site(s) on the WNV (+)3′SL RNA by deletion/mutation analyses. A deletion/mutation analysis was used to map additional regions on the WNV (+)3′SL RNA that interact with EF-1α. Ten mutated or deleted versions of the WNV (+)3′SL RNA (i.e., RNA-1) were generated and designated RNA-2 through RNA-11 (Fig. 8; Fig. 7A indicates the numerical positions of the nucleotides). Using nitrocellulose filter binding assays, the relative binding activity of each modified 3′SL RNA for EF-1α was compared to the binding activity of wild-type RNA-1 (Fig. 9A). The concentration of EF-1α was approximately 125 to 250 times higher than the concentration of the radiolabeled RNA probes in these experiments. Therefore, the slight differences in the probe concentrations were considered irrelevant under these assay conditions. RNA-2, which represents the bottom portion of RNA-1, retained 19% of the binding activity of RNA-1. RNA-3, which represents the top section of wild-type RNA-1 (5′-U_{47} to A_{97}-3′), retained 52% of the binding activity. This probe contained the protected region identified by the RNase footprinting experiment shown in Fig. 7. RNA-4 was created by deleting the smaller SL region, 5′-G_1 to G_{31}-3′, and this RNA retained 86% of the binding activity. RNA-5 was created by substituting 5′-$A_{67}G_{68}U_{69}G_{70}C_{71}$-3′, located in the top left loop, with 5′-$U_{67}C_{68}A_{69}C_{70}G_{71}$-3′. RNA-5 retained 82% of the binding activity. RNA-6 was created by changing the nucleotides in the top right loop from 5′-$U_{76}G_{77}U_{78}U_{79}A_{80}C_{81}$-3′ to 5′-$A_{76}C_{77}A_{78}A_{79}U_{80}G_{81}$-3′. These mutations in RNA-6 caused essentially no loss of binding activity. These data indicate the presence of multiple binding sites on the WNV (+)3′SL RNA. Over 50% of the binding activity of WNV (+)3′SL RNA was localized to the upper region of the main SL between 5′-U_{47} and A_{97}-3′, and approximately 18% of the binding activity of this region was contributed by the top left loop between 5′-A_{67} to C_{71}-3′. An additional low-activity binding site that contributed approximately 14% of the total binding activity was detected in the smaller SL consisting of 5′-G_1 to G_{31}-3′.

The proposed major binding site mapped by the RNase footprinting assay (see above) was further analyzed to determine the importance of this region in the interaction between EF-1α and WNV (+)3′SL RNA. The region between 5′-G_1 and G_{31}-3′ was deleted from all of the 3′SL RNA derivatives used in this experiment (Fig. 8, RNA-4 and RNA-7 to RNA-11) to eliminate the contribution of the small SL region to the total binding activity (i.e., approximately 14%), as determined by the previous experiment (Fig. 9A). For this nitrocellulose filter binding assay, RNA-4 was used as the control RNA for

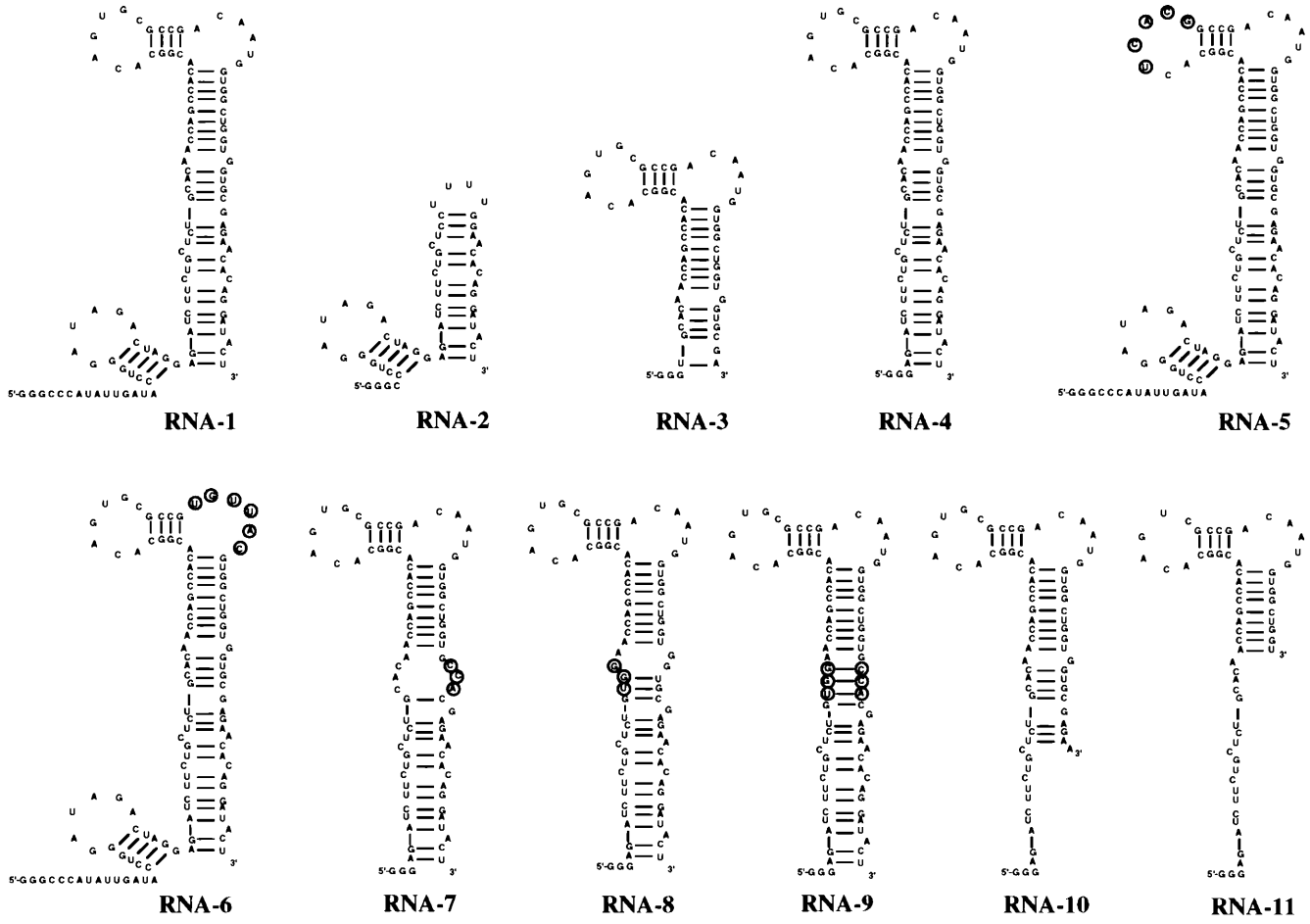

FIG. 8. Diagram of the WNV (+)3′SL RNA and its derivatives used for mapping EF-1α binding sites. ^{32}P-labeled WNV (+)3′SL RNA (RNA-1) and its derivatives (RNA-2 to RNA-11) were transcribed in vitro from DNA templates as described in Materials and Methods. Four uridine (U) residues were added to the sequence of RNA-2 to provide a loop at the top of the truncated stem (56). Mutated nucleotides are circled. RNA structures were predicted by the method of Zuker (69), using the FoldRNA program in the Genetics Computer Group sequence analysis software package (version 8). The structures of RNA-1 and RNA-2 were previously confirmed by structure probing (12, 56).

determining relative binding activity (Fig. 9B). RNA-7 was created by changing the sequence of nt 92 to 94 from 5′-$G_{92}U_{93}G_{94}$-3′ to 5′-$C_{92}C_{93}A_{94}$-3′, which prevents base pairing of the nucleotides in the region of the proposed major binding site. Nucleotides 92 to 94 are normally base paired with 5′-$C_{47}A_{48}C_{49}$-3′, which are the nucleotides that EF-1α protected in the RNase cleavage experiment (Fig. 7). Surprisingly, the binding activity of RNA-7 was 124% of that of RNA-4. RNA-8 was created by substituting nucleotides in the proposed major binding site from 5′-$C_{47}A_{48}C_{49}$-3′ to 5′-$U_{47}G_{48}G_{49}$-3′. Substitution of these nucleotides introduced mutations in the major binding site but retained base pairing at two of three positions compared to the wild-type RNA structure. RNA-8 retained only 40% of the binding activity of RNA-4. RNA-9 had the same mutations in the major binding site as RNA-8 and had complementary mutations on the other side of the stem to completely restore the double strandedness of the proposed major binding site. RNA-9 retained only 41% of the binding activity of RNA-4. RNA-10 and RNA-11 were created by deleting the 3′-terminal nucleotides 5′-A_{97} through U_{111}-3′ and 5′-U_{87} through U_{111}-3′, respectively. RNA-10 and RNA-11 retained 79 and 66%, respectively, of the binding activity of RNA-4.

These data suggest that the proposed major binding site on the WNV (+)3′SL RNA, nt 47 to 49, is involved in a direct interaction with EF-1α, since mutations in this region significantly reduced binding activity (Fig. 9B, RNA-8 and RNA-9). Deletion of the upper portion of the main stem (nt 47 to 97), which includes the major binding site, also caused a significant reduction in binding activity (Fig. 9A, RNA-2). Interestingly, the proposed major binding site exhibited increased binding activity when it was present in a single-stranded region rather than in a double-stranded region (Fig. 9B, RNA-7). Mutations in the top left loop caused a moderate reduction in the binding activity, suggesting that a minor binding site is located there (Fig. 9A, RNA-5). The smaller SL (nt 1 to 31) is also likely to contain a minor binding site, since deletion of this region also caused a moderate reduction in binding activity (Fig. 9A, RNA-4). Thus, the overall structural integrity of the WNV (+)3′SL RNA appears to be important for it to fully interact with EF-1α since none of the truncated 3′SL RNAs retained wild-type binding activity.

It was reported in previous filter binding studies that the EF-Tu · GTP complex, the bacterial homolog of the EF-1α · GTP complex, did not absorb to Millipore membranes in the presence of aminoacylated tRNA (aa-tRNA); however, loss of retention was not observed when nonaminoacylated tRNAs were used (reference 45 and references therein). A molecular explanation for the change in adsorption properties of the ternary complex (i.e., EF-Tu · GTP · aa-tRNA) is not

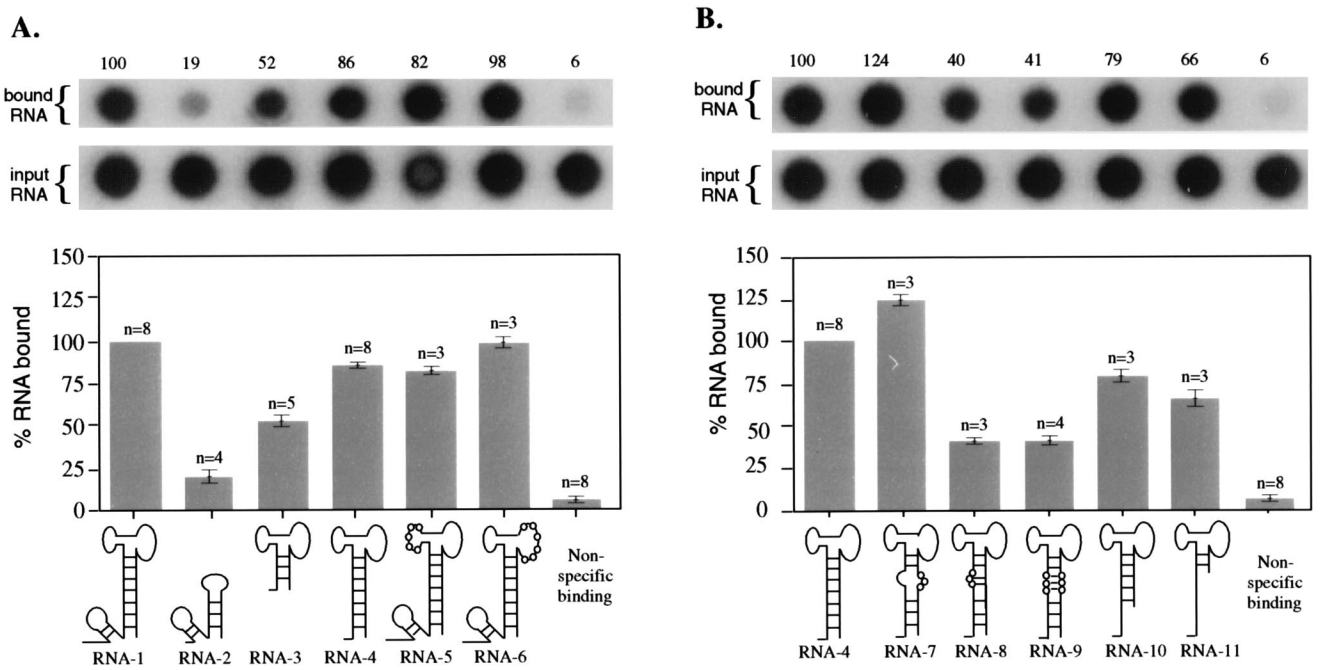

FIG. 9. Mapping regions on WNV (+)3′SL RNA that interact with EF-1α. The binding activities of RNA-1, -2, -3, -4, -5, and -6 (A) and of (B) RNA-4, -7, -8, -9, -10, and -11 (B) were compared in a nitrocellulose filter binding assay. The ^{32}P-labeled RNAs (approximately 80 to 160 pM, final concentration) were separately incubated with EF-1α (approximately 20 nM, final concentration) in a binding reaction mixture (100 μl) for 30 min. Ninety percent (90 μl) of each binding reaction mixture was vacuum filtered through a nitrocellulose membrane and washed with binding buffer. To calculate the amount of total input RNA used in each reaction, 10% (10 μl) of the binding reaction mixture was spotted on the nitrocellulose membrane and dried. The bound and total input [^{32}P]RNA that was retained on the nitrocellulose membrane is shown at the top of panels A and B. To determine the amount of nonspecific binding of [^{32}P]RNA to the nitrocellulose membrane, heat-inactivated EF-1α (see Materials and Methods) was substituted for active EF-1α in binding reaction mixtures (last spot in panels A and B). All of the [^{32}P]RNAs had similar nonspecific binding activities (±0.5% [data not shown]). The nitrocellulose membranes were phosphorimaged (Fujix BAS1000 phosphorimager), and the amount of radioactivity retained on the membrane for each binding reaction mixture was quantified by using MacBAS version 2.00 software. The number above each bound RNA spot indicates the relative percentage of each RNA species retained on the membrane. A graphical representation of the relative binding activities of the [^{32}P]RNAs is shown at the bottom of panels A and B. The binding activities of RNA-1 (A) and RNA-4 (B) were normalized to 100%, and the binding activities of the other RNAs were calculated relative to the normalized value. Error bars indicate the experimental variation. The number (n) of times the binding assays were repeated with each of the RNA species is indicated. A diagram of the RNA used for each binding reaction mixture is shown below the graphs, and the positions of substituted nucleotides are indicated by circles.

available (45). Even though the membrane and binding conditions used in the present study differed from those in the previous studies, the nitrocellulose membranes used for the filter binding assays (above) were stained with amino black in one experiment to determine the amount of protein adsorbed (data not shown). No significant differences were observed in the amount of protein retained on the membranes in the presence or absence of WNV (+)3′SL RNA or any of its mutated or truncated derivatives.

Interaction between EF-1α and genomic WNV RNA in infected cells. The experiments above describe interactions between purified EF-1α and WNV (+)3′SL RNA under in vitro conditions. Additional experiments were designed to ascertain whether EF-1α interacts with the WNV RNA in infected cells. Cytoplasmic S100 supernatants from mock- or WNV-infected cells were immunoprecipitated with the anti-EF-1α antibody, and the immunoprecipitates were analyzed by RT-PCR amplification using primers specific for the 3′-terminal 114 nt of the WNV genomic RNA. To eliminate the possibility of coimmunoprecipitation of EF-1α and viral RNA due to an interaction of EF-1α with ribosomes in viral polysomes, a 100,000 × *g* centrifugation step used to prepare the cytoplasmic S100 supernatants to remove preassembled ribosomal complexes. The expected RT-PCR product, which was 114 bp in length, was detected in the WNV-infected, S100 supernatant that was immunoprecipitated with the anti-EF-1α antibody (Fig. 10, lane 7). The 114-bp RT-PCR product was also detected in the nonimmunoprecipitated WNV-infected S100 supernatant that was used as a positive control for the RT-PCR analysis (Fig. 10A, lane 8). The 114-bp RT-PCR product was not detected in mock-infected S100 supernatants in the presence and absence of the anti-EF-1α antibody (Fig. 10A, lanes 2 and 3, respectively) or in the mock- and WNV-infected samples that were immunoprecipitated with protein A alone (Fig. 10A, lanes 1 and 6, respectively) or an irrelevant antibody (Fig. 10A, lanes 4 and 9, respectively). A restriction enzyme analysis was used to confirm that the 114-bp RT-PCR product contained the expected WNV sequence (Fig. 10B). *Bgl*II restriction enzyme digestion of the 114-bp RT-PCR product produced the expected 79- and 35-bp DNA fragments (Fig. 10B, lane 2). Sequence analyses confirmed that the 114-bp RT-PCR product contained the expected WNV sequence (data not shown). In conclusion, these results suggest that WNV genomic RNA interacts with the cytosolic fraction of EF-1α in vivo.

DISCUSSION

Characteristics of the interaction between EF-1α and WNV (+)3′SL RNA. This is the first report of the molecular identity of a host protein that interacts specifically with the 3′ SL of the WNV genomic RNA. The normal biological role of EF-1α · GTP is to facilitate the binding of aa-tRNA to the ribosome during translation (52). The interaction between EF-1α · GTP and aa-tRNA is GTP dependent due to a GTP-induced con-

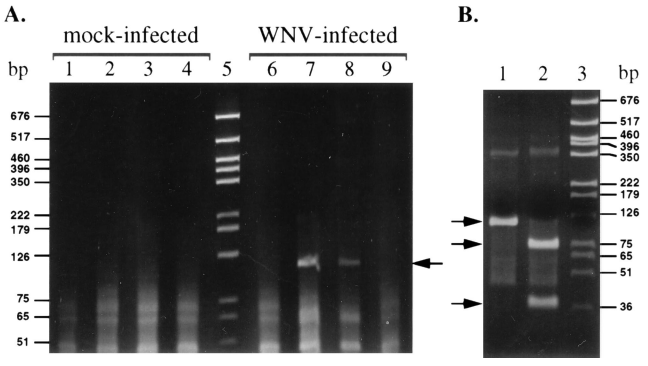

FIG. 10. Interaction between EF-1α and genomic WNV RNA in vivo. (A) RT-PCR was performed on S100 supernatants from mock-infected (lanes 1 to 4) and WNV-infected (lanes 6 to 9) BHK cells, using PCR primers that amplify the 114-bp region located at the 3′ terminus of the WNV genomic RNA. Lanes: 1 and 6, S100 supernatants immunoprecipitated with Sepharose A CL-4B beads alone (no antibody); 2 and 7, S100 supernatants immunoprecipitated with anti-EF-1α antibody coupled to Sepharose A CL-4B beads; 3 and 8, S100 supernatants prior to immunoprecipitation; 4 and 9, S100 supernatants immunoprecipitated with an unrelated goat antibody coupled to Sepharose A CL-4B beads. The sizes of the DNA markers (lane 5) are indicated on the left, and the arrow on the right indicates the position of the 114-bp RT-PCR product. (B) Restriction enzyme analysis of the 114-bp RT-PCR product. Lanes: 1, 114-bp RT-PCR product; 2, *Bgl*II digestion products of the 114-bp RT-PCR product; 3, DNA standards. The position of the 114-bp RT-PCR product (top arrow on left), the positions of the two *Bgl*II digestion products (bottom two arrows on left), and the sizes of the DNA markers (right) are indicated.

formational change in EF-1α (27). The release of an aa-tRNA from EF-1α to the ribosome coincides with the hydrolysis of the EF-1α-bound GTP. The resulting EF-1α · GDP complex is inactive and does not bind aa-tRNA until the GDP is replaced with GTP by other cellular proteins in the EF-1 complex (i.e., the EF-1 beta and delta subunits). Phosphorylation of EF-1α stimulates the rate of GDP-GTP exchange, which in turn promotes the formation of the EF-1α · GTP · aa-tRNA ternary complex (50). The data presented here indicate that phosphorylation of EF-1α is also required for its interaction with WNV (+)3′SL RNA (Fig. 5B) and may provide a mechanism for regulating the interaction between EF-1α and the viral genomic RNA during the WNV infection cycle. The high-affinity interactions between EF-Tu · GTP and its normal aa-tRNA substrates have equilibrium dissociation constants that are in the nanomolar range, i.e., 10^{-9} to 10^{-10} M (34, 47). The observed K_d (1.1 nM) for the interaction between EF-1α and WNV (+)3′SL RNA is in the same range as those reported between EF-Tu · GTP and aa-tRNAs. EF-Tu · GTP has been reported to interact with uncharged tRNA at lower affinity, approximately 10^{-7} M, which may explain why uncharged tRNA did not compete with the complex formed between WNV (+)3′SL RNA and EF-1α (Fig. 5A, lane 7) (54). Aminoacylation of tRNA is required for the high-affinity interaction with EF-1α · GTP but aminoacylation is not required for the interaction between EF-1α and WNV (+)3′SL RNA, suggesting that the viral RNA may contain recognition elements that mimic those of the aa-tRNA. Previous quantitative analyses demonstrated that EF-Tu interacts with aa-tRNA in a 1:1 molar ratio (5). In this study EF-1α was shown to interact with WNV (+)3′SL RNA in a 1.3:1 molar ratio, suggesting a similar stoichiometric relationship for the viral RNA-cell protein interaction.

Binding sites on the WNV (+)3′SL RNA for EF-1α. Previous analyses demonstrated that EF-Tu contains three domains (designated I, II, and III) (28). A recent crystallographic analysis of the ternary complex of EF-Tu, phenylalanylated tRNA ($tRNA^{Phe}$), and a GTP analog demonstrated that the aminoacylated 3′ end and the phosphorylated 5′ end of $tRNA^{Phe}$ bind at the interface between domains I and II and that the T arm binds to domain III (43). The high degree of sequence homology between prokaryotic EF-Tu and eukaryotic EF-1α make it likely that these proteins have similar structures and functional domains (1, 33, 44). The data available on the interaction between EF-1α and aa-tRNA also indicate that domains II and III of EF-1α interact with multiple sites on aa-tRNA; domain II binds to the aminoacyl group, and domain III binds to the anticodon of aa-tRNA (26). Similarly, the results from our RNase footprinting and nitrocellulose filter binding assays suggest that multiple interactions occur between EF-1α and the WNV (+)3′SL RNA (Fig. 6 and 8). Since the structure of the WNV (+)3′SL RNA does not show similarity to that of tRNA, and since the WNV (+)3′SL RNA cannot be aminoacylated, it is possible that the WNV (+)3′SL RNA interacts with EF-1α at sites that are distinct from those that are utilized by aa-tRNA. Experiments are in progress to determine whether aa-tRNA can function as a competitor of the WNV (+)3′SL RNA.

A region that accounted for approximately 60% of the overall EF-1α binding activity of the WNV (+)3′SL RNA was localized to 5′-$C_{47}A_{48}C_{49}$-3′ on the main stem of WNV (+)3′SL RNA. EF-1α interacted with this region in a sequence-specific manner and showed an increased binding activity for this region when it is single stranded (Fig. 9B, RNA-7). One possible explanation for this increase could be that the nucleotides in the major binding site were more accessible for interacting with EF-1α when they were bulged. Alternatively, the mutations may have induced an overall conformational change in the RNA structure that caused the increased reactivity with EF-1α. In addition to the high-activity binding site, two lower-activity binding regions were localized to the top loop (5′-$A_{67}G_{68}U_{69}G_{70}C_{71}$-3′) and in the smaller stem-loop (5′-G_1 to G_{31}-3′) of WNV (+)3′SL RNA (Fig. 9A). These low-activity sites may help to orient the interaction between EF-1α and WNV (+)3′SL RNA. The additive effects of both the high- and low-activity binding regions of the viral RNA appear to be required to obtain the overall activity and specificity of the observed interaction between EF-1α and WNV (+)3′SL RNA.

Translation factors involved in RNA virus replication. Translation factors have been shown to interact with the RNAs of some other positive-polarity RNA viruses (see the introduction) and have, in a few cases, been functionally associated with viral RNA synthesis. For example, the barley homolog of eIF-3 was shown to be associated with the BMV replication complex in vivo and enhanced BMV RNA synthesis in vitro (51). EF-Tu and EF-Ts were shown to be components of the active bacteriophage Qβ replicase complex (6, 31) and to play a fundamental structural role in the formation of stable Qβ replicase complexes (9). In addition to EF-Tu and EF-Ts, the Qβ replication complex also contains the ribosomal protein S1, which is required for template recognition during Qβ genome replication (10). Three host proteins (EF-1α, p84, and p105) have been shown to bind to the WNV (+)3′SL RNA (8). Although the Qβ and WNV systems utilize one common translation factor (EF-Tu/EF-1α), it is unlikely that p105 or p84 corresponds to S1 or EF-Ts, since there are no eukaryotic homologs for these two prokaryotic proteins with these molecular masses. The aminoacylated 3′-terminal tRNA-like structure of turnip yellow mosaic virus genomic RNA has previously been reported to bind EF-1α (25). Although these viral RNAs can be aminoacylated in vitro, no evidence has yet been obtained that aminoacylation plays a role in the viral replication cycle.

The data available on the host proteins that have been molecularly identified (see the introduction) suggest that different viruses may utilize unique sets of host proteins during replication.

Putative role(s) for EF-1α in WNV replication. The results from this study demonstrate that a soluble, cytoplasmic form of EF-1α can interact with the 3′ SL region of the WNV genomic RNA. It has been suggested that EF-1α attaches to the endoplasmic reticulum membrane via a posttranslational modification of the Asp^{306} residue (23). Similarly, we recently observed that an insoluble form of EF-1α colocalizes with the endoplasmic reticulum membrane fraction (data not shown) that was previously shown to contain the majority of the flavivirus RNA-dependent RNA polymerase activity (18, 21). Results from an additional study demonstrated that EF-1α can anchor mRNA to microtubules and actin filaments in vivo, suggesting that EF-1α is involved in sorting and regulating the expression of specific cellular mRNAs (4). It is possible that EF-1α is involved in targeting WNV RNA onto intracellular membranes that provide a microenvironment for the efficient replication of the viral RNA. In mammalian cells, the EF-1 complex is composed of four different subunits, alpha beta, gamma, and delta, in a molar ratio of 2:1:1:1 (14). In a similar manner, EF-1α may interact with viral proteins (e.g., viral polymerase) and/or other cellular proteins (e.g., p105 and p84) that bind to WNV (+)3′SL RNA. Instead of an enzymatic activity, EF-1α may provide protein-RNA and protein-protein interactions that promote the assembly of viral replication complexes.

Although the role of EF-1α in flavivirus replication remains to be determined, the specificity and high affinity of its interaction with WNV (+)3′SL RNA suggests that this interaction is functionally relevant to WNV infection. Furthermore, recent data indicate that EF-1α interacts with the structurally conserved 3′SL regions of the genomes of divergent flaviviruses, such as yellow fever virus, dengue virus type 2, and tick-borne encephalitis virus (8a). These results support a role for EF-1α in the replication of all flaviviruses. In addition, EF-1α has intrinsic characteristics that make it a suitable host protein for utilization in RNA virus replication. First, EF-1α is found in high concentrations in host cells. For instance, EF-1α represents approximately 1% of the total protein in animal cells and 5% in plant cells (13, 16). The abundance of EF-1α would make it unnecessary for viral replication to compete with cellular processes for limited amounts of the host protein. Second, EF-1α is highly conserved among different eukaryotic species. Since flaviviruses replicate in both invertebrate and vertebrate hosts, it is likely that host factors selected for virus replication would be both structurally and functionally conserved across different species. Third, the net positive charge (pI of approximately 9) (14) of EF-1α is characteristic of proteins that interact with negatively charged RNA. EF-1α affords an excellent model system for the further analysis of host protein-viral RNA interactions.

ACKNOWLEDGMENTS

We thank Cynthia A. Derdeyn for critical reading of the manuscript. We also thank David W. Speicher and David F. Reim (Wistar Institute Protein Microsequencing Facility, Philadelphia, Pa.) and Timothy M. Brown (GSU DNA/Protein Core Facility, Atlanta, Ga.) for analyzing and sequencing the EF-1α peptides.

This work was supported by Public Health Service research grants AI18382 from the National Institute of Allergy and Infectious Diseases and GM54896 from the National Institute of General Medical Sciences. Purchase of the DNA synthesizer (model 381; Applied Biosystems) and the protein sequencer (System Gold model; Beckman) was funded by the Georgia Research Alliance.

REFERENCES

1. **Amons, R., W. Pluijms, K. Roobol, and W. Moller.** 1983. Sequence homology between EF-1 alpha, the alpha-chain of elongation factor 1 from Artemia salina and elongation factor EF-Tu from Escherichia coli. FEBS Lett. **153:** 37–42.
2. **Ann, D. K., I. K. Moutsatsos, T. Nakamura, H. H. Lin, P. L. Mao, M. J. Lee, S. Chin, R. K. Liem, and E. Wang.** 1991. Isolation and characterization of the rat chromosomal gene for a polypeptide (pS1) antigenically related to statin. J. Biol. Chem. **266:**10429–10437.
3. **Barton, D. J., S. G. Sawicki, and D. L. Sawicki.** 1991. Solubilization and immunoprecipitation of alphavirus replication complexes. J. Virol. **65:**1496–1506.
4. **Bassell, G. J., C. M. Powers, K. L. Taneja, and R. H. Singer.** 1994. Single mRNAs visualized by ultrastructural *in situ* hybridization are principally localized at actin filament intersections in fibroblasts. J. Cell Biol. **126:**863–876.
5. **Bensch, K., U. Pieper, G. Ott, N. Schirmer, M. Sprinzl, and A. Pingoud.** 1991. How many EF-Tu molecules participate in aminoacyl-tRNA binding? Biochimie **73:**1045–1050.
6. **Biebricher, C. K., and M. Eigen.** 1988. Kinetics of RNA replication of Qβ replicase, p. 1–18. *In* E. Domingo, J. J. Holland, and P. Ahlquist (ed.), RNA genetics, vol. 1. CRC Press, Boca Raton, Fla.
7. **Black, A. C., J. Luo, C. Watanabe, S. Chun, A. Bakker, J. K. Fraser, J. P. Morgan, and J. D. Rosenblatt.** 1995. Polypyrimidine tract-binding protein and heterogeneous nuclear ribonucleoprotein A1 bind to human T-cell leukemia virus type 2 RNA regulatory elements. J. Virol. **69:**6852–6858.
8. **Blackwell, J. L., and M. A. Brinton.** 1995. BHK cell proteins that bind to the 3′ stem-loop structure of the West Nile virus genome RNA. J. Virol. **69:** 5650–5658.

8a. **Blackwell, J. L., and M. A. Brinton.** Unpublished data.

9. **Blumenthal, T.** 1980. Interaction of host-coded and virus-coded polypeptides in RNA phage replication. Proc. R. Soc. Lond. Ser. B **210:**321–335.
10. **Blumenthal, T., and G. G. Carmichael.** 1979. RNA replication: function and structure of Qbeta-replicase. Annu. Rev. Biochem. **48:**525–548.
11. **Brinton, M. A.** 1983. Analysis of extracellular West Nile virus particles produced by cell cultures from genetically resistant and susceptible mice indicates enhanced amplification of defective interfering particles by resistant cultures. J. Virol. **46:**860–870.
12. **Brinton, M. A., A. V. Fernandez, and J. H. Dispoto.** 1986. The 3′-nucleotides of flavivirus genomic RNA form a conserved secondary structure. Virology **153:**113–121.
13. **Browning, K. S., J. Humphreys, W. Hobbs, G. B. Smith, and J. M. Ravel.** 1990. Determination of the amounts of the protein synthesis initiation and elongation factors in wheat germ. J. Biol. Chem. **265:**17967–17973.
14. **Carvalho, J. F., M. D. Carvalho, and W. C. Merrick.** 1984. Purification of various forms of elongation factor 1 from rabbit reticulocytes. Arch. Biochem. Biophys. **234:**591–602.
15. **Chang, Y.-N., D. J. Kenan, J. D. Keene, A. Gatignol, and K.-T. Jeang.** 1994. Direct interactions between autoantigen La and human immunodeficiency virus leader RNA. J. Virol. **68:**7008–7020.
16. **Condeelis, J.** 1995. Elongation factor 1 alpha, translation and the cytoskeleton. Trends Biochem. Sci. **20:**169–170.
17. **D'Alessio, J. A.** 1982. RNA sequencing, p. 173–197. *In* D. Rickwood and B. D. Hames (ed.), Gel electrophoresis of nucleic acids. IRL Press, Oxford, England.
18. **Edward, Z., and T. Takegami.** 1993. Localization and functions of Japanese encephalitis virus nonstructural proteins NS3 and NS5 for viral RNA synthesis in the infected cells. Microbiol. Immunol. **37:**239–243.
19. **Gatignol, A., A. Buckler-White, B. Berkhout, and K.-T. Jeang.** 1991. Characterization of a human TAR RNA-binding protein that activates the HIV-1 LTR. Science **251:**1597–1600.
20. **Grange, T., M. Bouloy, and M. Girard.** 1985. Stable secondary structure at the 3′ end of the genome of yellow fever virus (17D vaccine strain). FEBS Lett. **188:**159–163.
21. **Grun, J. B., and M. A. Brinton.** 1987. Dissociation of NS5 from cell fractions containing West Nile virus-specific polymerase activity. J. Virol. **61:**3641–3644.
22. **Harris, K. S., W. Xiang, L. Alexander, W. S. Lane, A. V. Paul, and E. Wimmer.** 1994. Interaction of poliovirus polypeptide $3CD^{pro}$ with the 5′ and 3′ termini of the poliovirus genome. Identification of viral and cellular cofactors needed for efficient binding. J. Biol. Chem. **269:**27004–27014.
23. **Hayashi, Y., R. Urade, S. Utsumi, and M. Kito.** 1989. Anchoring of peptide elongation factor EF-1 alpha by phosphatidylinositol at the endoplasmic reticulum membrane. J. Biochem. **106:**560–563.
24. **Hayes, R. J., and K. W. Buck.** 1990. Complete replication of a eukaryotic virus RNA *in vitro* by a purified RNA-dependent RNA polymerase. Cell **63:**363–368.
25. **Joshi, R. L., J. M. Ravel, and A. L. Haenni.** 1986. Interaction of turnip yellow mosaic virus val-tRNA with eukaryotic elongation factor EF-1α. Search for a function. EMBO J. **5:**1143–1148.
26. **Kinzy, T. G., J. P. Freeman, A. E. Johnson, and W. C. Merrick.** 1992. A model for the aminoacyl-tRNA binding site of eukaryotic elongation factor-1

alpha. J. Biol. Chem. **267:**1623–1632.
27. **Kjeldgaard, M., P. Nissen, S. Thirup, and J. Nyborg.** 1993. The crystal structure of elongation factor EF-Tu from Thermus aquaticus in the GTP conformation. Structure **1:**35–50.
28. **Kjeldgaard, M., and J. Nyborg.** 1992. Refined structure of elongation factor EF-Tu from Escherichia coli. J. Mol. Biol. **223:**721–742.
29. **Kusov, Y., M. Weitz, G. Dollenmeier, V. Gauss-Muller, and G. Siegl.** 1996. RNA-protein interactions at the 3′ end of the hepatitis A virus RNA. J. Virol. **70:**1890–1897.
30. **Laemmli, U. K.** 1970. Cleavage of structural proteins during the assembly of the head of bacteriophage T4. Nature (London) **227:**680–685.
31. **Landers, T. A., T. Blumenthal, and K. Weber.** 1974. Function and structure in ribonucleic acid phage Qβ ribonucleic acid replicase. The roles of the different subunits in transcription of synthetic templates. J. Biol. Chem. **249:**5801–5808.
32. **La Vallie, E. R., J. M. McCoy, D. B. Smith, and P. Riggs.** 1994. Enzymatic and chemical cleavage of fusion proteins, p. 16.4.5–16.4.17. *In* F. M. Ausubel, R. Brent, R. E. Kingson, D. D. Moore, J. G. Seidman, J. A. Smith, and K. Struhl (ed.), Current protocols in molecular biology. Greene Publishing and Wiley-Interscience, New York, N.Y.
33. **Linz, J. E., L. M. Lira, and P. S. Sypherd.** 1986. The primary structure and the functional domains of an elongation factor-1 alpha from *Mucor racemosus*. J. Biol. Chem. **261:**15022–15029.
34. **Louie, A., N. S. Ribeiro, B. R. Reid, and F. Jurnak.** 1984. Relative affinities of all *Escherichia coli* aminoacyl-tRNAs for elongation factor Tu-GTP*. J. Biol. Chem. **259:**5010–5016.
35. **Lu, C. D., J. E. Houghton, and A. T. Abdelal.** 1992. Characterization of the arginine repressor from Salmonella typhimurium and its interactions with the carAB operator. J. Mol. Biol. **225:**11–24.
36. **Mandl, C. W., H. Holzmann, C. Kunz, and F. X. Heinz.** 1993. Complete genomic sequence of Powassan virus: evaluation of genetic elements in tick-borne versus mosquito-borne flaviviruses. Virology **194:**173–184.
37. **Men, R., M. Bray, D. Clark, R. M. Chanock, and C.-J. Lai.** 1996. Dengue type 4 virus mutants containing deletions in the 3′ noncoding region of the RNA genome: analysis of growth restriction in cell culture and altered viremia pattern and immunogenicity in rhesus monkeys. J. Virol. **70:**3930–3937.
38. **Mohan, P. M., and R. Padmanabhan.** 1991. Detection of stable secondary structure at the 3′ terminus of dengue virus type 2 RNA. Gene **108:**185–191.
39. **Moos, M.** 1994. Isolation of proteins for microsequence analysis, p. 10.19.1–10.19.12. *In* F. M. Ausubel, R. Brent, R. E. Kingson, D. D. Moore, J. G. Seidman, J. A. Smith, and K. Struhl (ed.), Current protocols in molecular biology. Greene Publishing and Wiley-Interscience, New York, N.Y.
40. **Nakhasi, H. L., X. Q. Cao, T. A. Rouault, and T. Y. Lui.** 1991. Specific binding of host cell proteins to the 3′-terminal stem-loop structure of rubella virus negative-strand RNA. J. Virol. **65:**5961–5967.
41. **Nakhasi, H. L., T. A. Rouault, D. J. Haile, T. Y. Lui, and R. D. Klausner.** 1990. Specific high-affinity binding of host cell proteins to the 3′ region of rubella virus RNA. New Biol. **2:**255–264.
42. **Nakhasi, H. L., N. K. Singh, G. P. Pogue, X. Q. Cao, and T. A. Rouault.** 1994. Identification and characterization of host factor interactions with *cis*-acting elements of rubella virus RNA. Arch. Virol. Suppl. **9:**255–267.
43. **Nissen, P., M. Kjeldgaard, S. Thirup, G. Polekhina, L. Reshetnikova, B. F. Clark, and J. Nyborg.** 1995. Crystal structure of the ternary complex of phe-tRNA^{phe}, EF-Tu, and a GTP analog. Science **270:**1464–1472.
44. **Nordnes, S., S. Krauss, and T. Johansen.** 1994. cDNA sequence of zebrafish (Brachydanio rerio) translation elongation factor-1 alpha: molecular phylogeny of eukaryotes based on elongation factor-1 alpha protein sequences. Biochim. Biophys. Acta **1219:**529–532.
45. **Ofengand, J.** 1974. Assay for aa-tRNA recognition by the EFTu-GTP complex of Escherichia coli. Methods Enzymol. **29:**661–667.
46. **O'Neill, R., and P. Palese.** 1994. *Cis*-acting signals and *trans*-acting factors involved in influenza virus RNA synthesis. Infect. Agents Dis. **3:**77–84.
47. **Ott, G., M. Schiesswohl, S. Kiesewetter, C. Forster, L. Arnold, V. Erdmann, and M. Sprinzl.** 1990. Ternary complexes of *Escherichia coli* aminoacyl-tRNAs with the elongation factor Tu and GTP: thermodynamic and structural studies. Biochim. Biophys. Acta **1050:**222–225.
48. **Palen, E., T. T. Huang, and J. A. Traugh.** 1990. Comparison of phosphorylation of elongation factor 1 from different species by casein kinase II. FEBS Lett. **274:**12–14.
49. **Pardigon, N., and J. H. Strauss.** 1996. Mosquito homolog of the La autoantigen binds to Sindbis virus RNA. J. Virol. **70:**1173–1181.
50. **Peters, H. I., Y. W. Chang, and J. A. Traugh.** 1995. Phosphorylation of elongation factor 1 (EF-1) by protein kinase C stimulates GDP/GTP-exchange activity. Eur. J. Biochem. **234:**550–556.
51. **Quadt, R., C. C. Kao, K. S. Browning, R. P. Hershberger, and P. Ahlquist.** 1993. Characterization of a host protein associated with brome mosaic virus RNA-dependent RNA polymerase. Proc. Natl. Acad. Sci. USA **90:**1498–1502.
52. **Riis, B., S. I. Rattan, B. F. Clark, and W. C. Merrick.** 1990. Eukaryotic protein elongation factors. Trends Biochem. Sci. **15:**420–424.
53. **Sambrook, J., E. F. Fritsch, and T. Maniatis.** 1989. Molecular cloning: a laboratory manual, 2nd ed. Cold Spring Harbor Laboratory Press, Cold Spring Harbor, N.Y.
54. **Schulman, R. G., C. W. Hilbers, and D. L. Miller.** 1974. Nuclear magnetic resonance studies of protein-RNA interactions. I. The elongation factor Tu-GTP aminoacyl-tRNA complex. J. Mol. Biol. **90:**601–607. (Letter.)
55. **Shenolikar, S.** 1994. Analysis of protein interactions, p. 18.0.1–18.6.19. *In* F. M. Ausubel, R. Brent, R. E. Kingson, D. D. Moore, J. G. Seidman, J. A. Smith, and K. Struhl (ed.), Current protocols in molecular biology. Greene Publishing and Wiley-Interscience, New York, N.Y.
56. **Shi, P. Y., M. A. Brinton, J. M. Veal, Y. Y. Zhong, and W. D. Wilson.** 1996. Evidence for the existence of a pseudoknot structure at the 3′ terminus of the flavivirus genomic RNA. Biochemistry **35:**4222–4230.
57. **Singh, N. K., C. D. Atreya, and H. L. Nakhasi.** 1994. Identification of calreticulin as a rubella virus RNA binding protein. Proc. Natl. Acad. Sci. USA **91:**12770–12774.
58. **Springer, T. A.** 1994. Purification of proteins by precipitation, p. 10.16.1–10.16.11. *In* F. M. Ausubel, R. Brent, R. E. Kingson, D. D. Moore, J. G. Seidman, J. A. Smith, and K. Struhl (ed.), Current protocols in molecular biology. Greene Publishing and Wiley-Interscience, New York, N.Y.
59. **Sriskanda, V. S., G. Pruss, X. Ge, and V. B. Vance.** 1996. An eight-nucleotide sequence in the potato virus X 3′ untranslated region is required for both host protein binding and viral multiplication. J. Virol. **70:**5266–5271.
60. **Takegami, T., M. Washizu, and K. Yasui.** 1986. Nucleotide sequence at the 3′ end of Japanese encephalitis virus genome RNA. Virology **152:**483–486.
61. **Vaheri, A., W. D. Sedwick, S. A. Plotkin, and R. Maes.** 1965. Cytopathic effect of rubella virus in BHK-21 cells and growth to high titers in suspension cultures. Virology **27:**239–241.
62. **Venema, R. C., H. I. Peters, and J. A. Traugh.** 1991. Phosphorylation of elongation factor 1 (EF-1) and valyl-tRNA synthetase by protein kinase C and stimulation of EF-1 activity. J. Biol. Chem. **266:**12574–12580.
63. **Venema, R. C., H. I. Peters, and J. A. Traugh.** 1991. Phosphorylation of valyl-tRNA synthetase and elongation factor 1 in response to phorbol esters is associated with stimulation of both activities. J. Biol. Chem. **266:**11993–11998.
64. **Wallner, G., C. W. Mandl, C. Kunz, and F. X. Heinz.** 1995. The flavivirus 3′-noncoding region: extensive size heterogeneity independent of evolutionary relationships among strains of tick-borne encephalitis virus. Virology **178:**169–178.
65. **Weeks, K. M., and D. M. Crothers.** 1992. RNA binding assays for Tat-derived peptides: implications for specificity. Biochemistry **31:**10281–10287.
66. **Wengler, G., and E. Castle.** 1986. Analysis of structural properties which possibly are characteristic for the 3′-terminal sequence of the genome RNA of flaviviruses. J. Gen. Virol. **67:**1183–1188.
67. **Wilusz, K. M., M. G. Kurilla, and J. D. Keene.** 1983. A host protein (La) binds to a unique species of minus-sense leader RNA during replication of vesicular stomatitis virus. Proc. Natl. Acad. Sci. USA **80:**5827–5831.
68. **Yu, W., and J. L. Leibowitz.** 1995. A conserved motif at the 3′ end of mouse hepatitis virus genomic RNA required for host protein binding and viral RNA replication. Virology **214:**128–138.
69. **Zuker, M.** 1989. Computer prediction of RNA structure. Methods Enzymol. **180:**262–288.